 DOI: 10.1002/masy.200650511

The Swelling Behavior of Charged Hydrogels

Bernward A. Mann,[1] *Kurt Kremer,*[1] *Christian Holm*[1,2]

Summary: We describe recent advances obtained in understanding the microscopic interplay of a charged hydrogel with its confined mobile counterions. Results of extensive computer simulations are compared to simple scaling descriptions for various solvent conditions. We will briefly discuss our simulation package ESPResSo which was used to perform the simulations. We demonstrate why simple scaling theories suffice to adequately describe the swelling behavior of these systems despite their enormous complexity. We will conclude with a presentation of ongoing results for polyelectrolyte networks under poor solvent conditions.

Keywords: computer modeling; hydrogels; molecular dynamics; polyelectrolytes; solution properties

1 Introduction

For quite some time now computer simulations have been established as an efficient methodology which connects theoretical treatments and real-world experiments, particularly for very complex systems. They allow for well-defined systems (no impurities, parasitic drag, ...) which can be thoroughly evaluated and analyzed without much problems, since all real-world observables are available from the direct access to all microscopical details of the ''experiment''. This also allows control over individual effects by systematically manipulating environmental or particle parameters to study their impact on the entire ensemble, giving valuable insight into what the leading contributions and mechanisms are that govern the macroscopic behavior of the sample. Ideally, the results then enable experimentalists to focus their efforts on optimizing only predominantly important ingredients in their setup, control primary sources of error, and develop measurement methods for isolating the main effects, while theoreticians are given some means to evaluate the proposed models, whether their predictions can be confirmed quantitatively or at least qualitatively, and the validity of the underlying assumptions, whether these apply to the considered parameter regimes or need to be adjusted or revised. Here, another advantage of computer simulations becomes obvious: Being simplified descriptions of reality themselves, they can be based on the very same assumptions the theoretical models impose, consequently revealing how the latter would behave as real world systems but representing an idealized realization of the experimental system at the same time. This bridges the gap between theory and experiment by determining how the systems *would* behave experimentally if all the theoretical model assumptions and simplifications were correct; any deviations found can then be traced rather easily[1] to imperfections in the underlying description of reality, be it that

[1] Max-Planck-Institut für Polymerforschung, Ackermannweg 10, 55128 Mainz, Germany; Fax: (+49) 6131 379100; Email: {mann, holm, kremer}@mpip-mainz.mpg.de

[2] Frankfurt Institute for Advanced Studies (FIAS), Max–von–Laue–Straße 1, 60438 Frankfurt, Germany, Fax: (+49) 69 79847611; Email: C.holm@fias.uni-frankfurt.de

[1] At least compared to the effort it would take the experimentalists to improve on their measurements, trying to separate interacting effects and to isolate microscopic details in a macroscopic sample, or to the problems theoreticians would have to face if they had to relinquish several of their (well-justified) presumptions about the system.

© 2006 WILEY-VCH Verlag GmbH & Co. KGaA, Weinheim

WILEY InterScience®

some of the simplifications were unjustified or too extensive, that important aspects or contributions were wrongfully neglected, or that the modeling itself failed to depict the leading mechanisms correctly. Next, whatever changes are proposed can directly be executed within the simulation environment, introducing new or modifying existing constraints, adding extended functionality or degrees of freedom if necessary (e.g. dipolar moments or rotational orientations, which are both commonly neglected), or simply evaluating the different model components separately to determine if their significance was properly addressed by the theory. Particularly the latter usually leads to the most valuable insight computer simulations can offer: While the analytical treatment concentrates on the description of certain aspects of the system and aims for explicit predictions of selected observables, the simulation reveals the full behavior of (a simplified version of) the setup and obtains complete particle trajectories and their spatio-temporal evolution (which themselves need to be analyzed as any experimental data has to be); but because both are based on the same model assumptions, comparing forecast and observation, then investigating how deviations change when manipulating model mechanisms in the simulation allows specific statements about their theoretical treatment and any changes necessary therein. Although it will always depend on the verification through ''real'' experiments and to no lesser extend on the input and guidance by analytical studies, the methodology of computational investigations has proved its worth over the years particularly in such complex and challenging applications as the many-body macromolecular systems in polymer physics with their different time and length scales, layers of intertwined interactions and coarse-grained behavior based on microscopic details.

In this contribution we will present the computer simulation package ESPResSo an **E**xtensible **S**imulation **P**ackage for **Res**earch on **S**oft Matter Systems [1, 2], which was created and written by A. Arnold, H.-J. Limbach, and B.A. Mann at the theory division of the Max-Planck-Institute for Polymer Research. Presenting the programs design, capabilities, and core features in section 2, we are afterwords addressing as an application of ESPResSo the swelling behavior of polyelectrolyte networks. Section 3.1 is thereby introducing the model used to represent charged hydrogels in different solutions, giving a detailed analysis of the pressure contributions balancing the swelling equilibrium of a good solvent in section 3.2, while illustrating the conformational changes occurring when the networks can no longer be treated as hydrophilic due to poor solvent conditions in section 3.3.

2 ESPResSo – An Extensible Simulation Package for the Research on Soft Matter Systems

Soft matter is a term for materials in states that are neither simple liquids nor hard solids (crystals, ...) but rather macromolecular assemblies, e.g. polymers, colloids, liquid crystals, and dipolar fluids. Many such materials are familiar from everyday life – glues, paints, soaps, baby diapers – while others are important in industrial processes, such as polymer melts that are molded and extruded to form plastics [3], or polymer networks for the development of rubber [4]. Biological components are mainly made out of soft matter as well, *i.e.* DNA, membranes, filaments and other proteins, and even most of the food we digest belongs to this class.

Common for all these materials is the importance of a wide range of length and time scales for both their microscopic behavior and their macroscopic properties. Since typical energies between different structures are similar to thermal energies, Brownian motion of thermal fluctuations plays a prominent role. Another key feature, the propensity of soft matter systems to self-assemble, often results in complex phase behaviors yielding a rich variety of accessible structures; most of the biological

© 2006 WILEY-VCH Verlag GmbH & Co. KGaA, Weinheim

systems are not even in equilibrium usually but evolve along switchable steady states. Much of today's insight into their underlying mechanisms has thereby been gained through computer simulations of these systems at either the full atomistic or on a coarse-grained, so called *mesoscopic*, level.

In the past, charged polymers (polyelectrolytes) and colloids have been a key center of interest in the research activities at our institute. Serving as important substances for many of the technical applications mentioned so far, charged systems also occur in biological environments [5] and are already involved when modeling explicit water, hereby entering through the partial charges. Simulating these systems is not straightforward and very time consuming [6, 7, 8], since the effort scales at best linearly with the number of charges, thus the production of single data points could take weeks or even months for complex biomolecular problems [9]. Consequently, a number of algorithms have been improved or developed in our group which yield fast expressions for the energy and forces of fully or partially periodic systems [10, 11, 12, 13, 14], pending a suitable simulation environment to be applied to. Another research focus in our group, besides considering charged systems in various geometries, e.g. films or porous media, and with different topologies ranging from linear to branched to networks [15, 16], considers systematically coarse-graining atomistic models such that one can access mesoscopic time and length scales with computer simulations [17, 18, 19], necessary for *quantitatively* predicting dynamic properties or surface interactions for complex materials which depend on local chemical interactions and local packing. For the coarse-graining procedure it is required to switch back and forth between an atomistic and a coarse-grained description, implying complicated steering schemes for a simulation; therefore, a high flexibility of the steering level and an easy way to interact with other programs is needed as well as extensibility to easily implement and test new methods and algorithms, because such tasks usually involve changes in the core part of a program.

What else should a suitable program be able to do? It should be easy to use, but scientifically sound; it should grant experts access to advanced algorithms and techniques, but enable beginners to investigate scientific problems easily and at the same time not limit them to run the program as a ''black box''; it should be general and flexible, but still fast; it should be easily extensible, but remain at the same time reliable and keep continuity with older versions.

These were the guidelines in the development of ESPResSo İt is tailored to study soft matter model systems via Molecular Dynamics (MD) algorithms, with particular emphasis on extensibility for new, highly complex force/energy algorithms. Since a full description of the program is given in [2], we will limit ourself to a quick overview in this section.

ESPResSo is organized in two hierarchical program levels, each suited to optimize some of the main targets in mind: the *steering level* for large flexibility, usability and user-defined extensibility, the *simulation engine level* for efficiency, readability and package-wide extensibility. The steering of ESPResSo is done on a script language level, namely Tcl/Tk[20], where all tasks (such as input and output of data, setting of particle properties, interactions, and parameters, and performing the integration and analysis of a given system) are implemented as C-functions enhancing the Tcl-interpreter and acting as new Tcl-script commands, which are by construction able to both set and retrieve informations similar to the Tcl-syntax. From the steering level one can interact with the actual simulation in a very flexible way, meaning that one can change the system properties during the simulation in any desired way, may this be the insertion or deletion of particles, a change of interaction parameters, a switch from one to another thermodynamic ensemble, a change of parameters for the integrator or the thermostat – just to name a few possibi-

© 2006 WILEY-VCH Verlag GmbH & Co. KGaA, Weinheim

lities. As all these steps described are typically part of the Tcl-script that steers the simulation, even more complex tasks can easily be formulated with the Tcl language, although for performance reasons it might always be better to consider implementing commonly used and/or time-critical features within the much faster C-core of the simulation engine level which is designed to be as efficient as possible, being responsible for storing the particle and interaction data on any number of processors, but also performing the integration of Newton's equation of motion as well as the necessary calculations of basic quantities like forces, energies and pressures. The simulation engine code has been organized to be as modular as possible, separating clearly different tasks for better readability and accessibility, e.g. hiding the details of the complex numerical algorithms behind basic functions through well-defined lean interfaces. Also new potentials may be added to ESPResSo without touching the integrator code, while in turn the integrator can be modified without touching the potential implementations, rendering it much easier to implement a new type of interaction, a new integrator, or a new thermostat, as well as to understand as a user what the program is doing during the simulation – which is important in light of our belief that it is not useful to perform scientific research with a simulation tool that appears mainly as a ''black-box'' to the scientist utilizing it.

ESPResSo uses as default the *Velocity Verlet Molecular Dynamics integrator* [21, 22] for rotationally invariant particles, which is robust enough for most applications. If a simulation incorporates particles with rotationally degrees of freedom like dipoles or cigar shaped Lennard–Jones particles, the rotational degrees of freedom are represented by quaternions, and an extension of the velocity Verlet algorithm for rigid body motion is used [23]. Mass and inertia moments are fully implemented, but may be replaced by the default reduced mass $m^* = 1.0$ for performance reasons if no distinction of different masses is desired. For the simulation of dynamic experiments like a simple shear flow, the velocity Verlet integrator features a *Non Equilibrium Molecular Dynamics* (NEMD) integration scheme [24, 25]. In addition to the intrinsic (N, V, E)-ensemble, the velocity Verlet integrator can be combined with one of the implemented thermostats to obtain a (N, V, T)-ensemble. At the moment this includes a *Langevin thermostat*, a *Berendsen thermostat* [26] and a *dissipative particle dynamics thermostat* (DPD) [27, 25]. The type and the temperature of the thermostat can be changed during the simulation on the script level, allowing e.g. simulated annealing. Apart from (N, V, E)- and (N, V, T)-ensembles, the velocity Verlet integrator is also able to keep the pressure constant, i.e. to simulate the (N, p, T)*-ensemble* [28]. This is implemented by introducing an artificial piston mass which acts on the simulation box and rescales its dimensions isotropically. In addition to the implementation given in [28], our algorithm allows for using a constant tension ensemble as well, where only the pressure in one or two dimensions is considered, the rescaling adjusted to respond accordingly; this is useful when studying e.g. membranes under tension [29].

ESPResSo distinguishes three kinds of forces: short-ranged forces, long-ranged forces, and bonded interactions. Currently, only short-ranged pair-interactions are implemented, i.e. the *Lennard–Jones*, *Buckingham*, and *Gay–Berne potential*, plus some custom interactions such as the possibility to have arbitrary *tabulated potentials*; however, extending ESPResSo to three or more body forces is easily possible if the need arises. The bonded interactions are treated together with the short-ranged interactions, having no limitation on the number of bond partners (*i.e.* many-body bonded interactions are already implemented in ESPResSo). The calculation of long-ranged interactions requires much more care due to the large number of possible interaction partners, which is why algorithms for long-range interactions are highly sophisticated [7] and normally have their own parallelization strategies, separate from the one

© 2006 WILEY-VCH Verlag GmbH & Co. KGaA, Weinheim

applied to all other parts of the program. This enormous effort is justified by the fact that a simulation with e.g. electrostatic interactions might spend more than two thirds of the computation time only for the calculation of the long-range interactions. While ESPResSo initially focused on Coulomb interactions only [10, 11], since this is the dominant force for soft matter problems, fast algorithms for dipolar interactions have meanwhile been implemented as well as special routines to treat long-ranged forces in systems with partial periodicity with the utmost efficiency [12, 30, 31], too.

ESPResSo does not only supply the simulation kernel, but provides tools for analyzing the data as well. The analysis can be done both after the simulation is complete (''off-line''), or while it is running (''on-the-fly'') and the trajectory is still being built. This can be used to implement some simple plausibility checks, e.g. for following energy conservation or the temporal evolution of selected observables, allowing to abort the simulation in the case of abnormal values, or it may be employed to fully automize one's investigations such that at the end of the run the main observables are already analyzed and processed into ready-to-use, gnuplot-exported PostScript-plots.

To convey a feeling for the broad range of features already implemented in ESPResSo, this section gave details about some selected ones. By no means comprehensive, it is perhaps the part of the program growing quickest due to continuous contributions from developers and collaborators. Therefore, an up-to-date listing can always be found in the RELEASE_NOTES-file of the distribution and on our webpage (http://www.espresso.mpg.de) where you can also find further informations regarding content and obtainability of the package.

3 Polyelectrolyte Networks at Swelling Equilibrium

One of the most prominent features of a polyelectrolyte network can be observed when immersing a dry sample in solution: This hydrogel is then able to absorb large amounts of the solvent molecules, up to several hundred times its dry mass, while swelling to an enormous size. It will also respond to variations of the external conditions by rather drastic volume changes. Such remarkable properties allow numerous industrial applications, e.g. as superabsorbants (hygiene products, health care, water treatment, environmental cleanup operations), in drug delivery, cosmetics, pharmaceuticals, agriculture, in everyday products like rubber and compact discs, or as actuators in microfluidic devices [32, 33, 34, 35, 36, 37].

Chemically, charged hydrogels are composed of cross-linked polyelectrolytes, polymer chains which dissociate ions in polar solvents [38]. Due to the macroscopic requirement of electro-neutrality the counterions released from the chains are hereby confined inside the gel and exert an osmotic pressure which leads to the swelling of the network against the elastic response of the network strands. The increase of the counterion entropy caused by the larger volume available to the ions in the swollen state is thought to be the driving force behind the large swelling capacity of charged gels, neglecting long-range electrostatics, short-range hydrophobic interactions, and deviations from ideal behaviour. It is their delicate balance which renders the magnitude of the swelling and the phase behaviour of polyelectrolyte networks hard to predict [39].

Over the past decades, the attention polyelectrolyte networks attracted from both science and industry increased profoundly. While the latter used the gels' unprecedentedly high swelling capacity and their behaviour under external stimuli, the former's interest focuses on the complex interplay of short- and long-range effects which determine the equilibrium swelling properties [39]. Experimentally those have been extensively studied for a long time [40, 41, 42], where initial work concentrated on the swelling behaviour in solutions of simple salt [43, 44]. More recent studies

© 2006 WILEY-VCH Verlag GmbH & Co. KGaA, Weinheim

also addressed, among others, the influence of oppositely charged surfactants [45, 46, 47, 48, 49] and microgel particles [50, 51]. Theoretical approaches concentrated on thermodynamic arguments, developing rather simple models for the equilibrium states of charged gels [52, 53, 54], studying the swelling of polyelectrolyte and polyampholyte networks in pure solvent, in the presence of salt, in mixed solvents, and in the presence of other macroions, e.g. surfactant micelles [39]. They usually calculated the free energy of the gel as sum of contributions from the elasticity of the strands, the solvent interaction of the network, the free motion of the counterions (entropy term), and the electrostatics in the system.

Recently, numerical studies of polyelectrolyte networks [55, 56, 57, 58, 15, 16, 59] began to examine simple model systems, usually an end-to-end crosslinked gel with ideal diamond configuration in a (N, V, T)-ensemble at various network packing fractions and different sets of parameters [55, 57, 58] or in cubic symmetry and with explicit solvent [56] in very small systems, confirming the tremendous swelling as compared to uncharged systems [55, 58] and claiming a discontinuous volume transition at very high electrostatic coupling [57], but without investigating the connection of the measured data to the theoretical predictions mentioned before.

Here, we focus on the pressure contributions leading to the swelling equilibrium of the charged hydrogels (section 3.2), and analyze the conformational behaviour of polyelectrolyte networks placed in a poor solvent (section 3.3).

3.1 Simulation Model and Methods

In our simulations, we employ a perfect and defect-free network of N_p polyelectrolyte chains connected at their ends to N_{nodes} tetra-functional cross-linking sites (nodes); this network topology is conserved at all times. The polymer chains are modeled as bead spring chains of N_m Lennard-Jones (LJ) particles each with the FENE (Finite Extension Nonlinear Elastic) potential $U_{FENE}(r) = -\frac{1}{2}k_F r_F^2 \ln[1-(\frac{r}{r_F})^2]$ for $r \le r_F$ added for bonds and cross-links; the parameters are $k_F = 10.0\frac{k_BT}{\sigma^2}$, $r_F = 1.5\sigma$ [57] for good and θ-solvent, $k_F = 7.0\frac{k_BT}{\sigma^2}$, $r_F = 2.0\sigma$ [60] for poor solvent conditions, where σ is the monomer diameter (LJ unit). The van der Waals interaction between chain beads is modeled by the standard LJ potential vanishing for distances $r > r_c$ (the potential cut-off), while reading $U_{LJ}(r) = 4\varepsilon_{LJ}[(\frac{\sigma}{r})^{12} - (\frac{\sigma}{r})^6 - c]$ for shorter distances; the constant $c = (\frac{\sigma}{r_c})^{12} - (\frac{\sigma}{r_c})^6$ is chosen such that the potential value is zero and continuous in $r = r_c$. Good solvent is modeled by $r_c = 2^{1/6}\sigma$ and $\varepsilon_{LJ} = 1\ k_BT$, leaving only the repulsive part of the interaction; this potential is also employed for the mutual bead-counterion and counterion-counterion excluded volume interaction. The θ-solvent is modeled by an attractive interaction between the beads, represented by the same LJ potential, now with a larger cut-off ($r_c = 2.5\sigma$) and $\varepsilon_{LJ} = 0.34\ k_BT$ chosen to give θ-solvent properties [2], while the poor solvent conditions are mimiced by using $r_c = 2.5\sigma$ and $\varepsilon_{LJ} = 1.75\ k_BT$ between the monomers.

All counterions, the N_{nodes} nodes, and a fraction f of the N_m monomers on each of the N_p chains bear $q_i = \pm 1$ unit charges, interacting via the Coulomb energy $E_C(r_{ij}) = k_BT\ell_B q_i q_j / r_{ij}$ with other charged particles at distance r_{ij}, where the Bjerrum length $\ell_B = e^2/(4\pi\varepsilon_0\varepsilon_S k_BT)$ (e: unit charge, ε_0 and ε_S: permittivity of the vacuum and of the solvent, respectively) is defined as the distance at which two unit charges have an interaction energy of k_BT (*e.g.* for water $\ell_B = 7.1$ Å). The Coulomb interaction is calculated with the P3M-algorithm [10], tuned to force accuracies well above the thermal noise level.

The initial setup of the cubic simulation box with periodic boundary conditions has

[2] This value for ε_{LJ} was determined by U. Micka [61, 62] for a slightly different bond potential with $k_F = 7\frac{k_BT}{\sigma^2}$, $r_F = 2\sigma$; within the accuracy of the determination of θ we do not expect any deviation.

© 2006 WILEY-VCH Verlag GmbH & Co. KGaA, Weinheim

$N_p = 16$ polymer chains placed along the edges of a diamond lattice and connected at $N_{nodes} = 8$ tetra-functional nodes, a fraction of f monomers charged on each chain, and $N_{CI} = N_{nodes} + N_p \cdot fN_m$ counterions added to the system at random positions, ensuring overall electro-neutrality for the $N_{tot} = N_{nodes} + N_p \cdot N_m + N_{CI}$ particles (see Figure 1).

For the non-hydrophobic systems, we used the stochastic MD integration scheme for isothermal-isobaric (N, p, T)-ensembles metioned in section 2 with resonance coupling $\Omega_0 = \omega_0$ to the typical molecular frequency ω_0 deducible from the intermolecular potentials [28]. We chose $\gamma_0 = \tau^{-1} = \gamma_V/Q$ and $Q = 1/(\omega_0^2 V \kappa_T)$ for the remaining parameters [16] which adjusts the artificial piston mass Q of the algorithm such that sufficiently fast relaxation of the simulation box volume V to the equilibrium $V_{eq} = V(\mathcal{P} \approx P = 0)$ is achieved without unwanted ''box ringing'' [28]. Hereby, the ''instantaneous pressure'' $\mathcal{P}$ was measured using [28, 63]

$$\mathcal{P} = \rho k_B T - \frac{1}{3V} \sum_{i<j} \langle \vec{r}_{ij} \vec{f}_{ij}^{\,sr} \rangle + \frac{1}{3V} \langle E_C \rangle \quad (1)$$

(with $\vec{f}_{ij}^{\,sr}$ being all short-range forces, and $\langle E_C \rangle$ as averaged electrostatic energy), indicating if the fully periodic system prefered to expand ($\mathcal{P} > 0$) or to collapse ($\mathcal{P} < 0$). From there, the equilibrium properties of the swollen hydrogel were determined by switching to the (N, $V = V_{eq}$, T)-ensemble and applying a standard velocity Verlet algorithm, coupled to a heat bath and background friction (Langevin thermostat; friction coefficient $\Gamma = \tau^{-1}$, $T^* = 1\,\varepsilon/k_B T$). We integrated the equations of motion for 2400τ with timestep $\Delta t = 0.012\tau$ [64, 6].

It is alternatively also possible to *estimate* the final volume V_{eq} from the ideal gas law statement that the energy PV is conserved

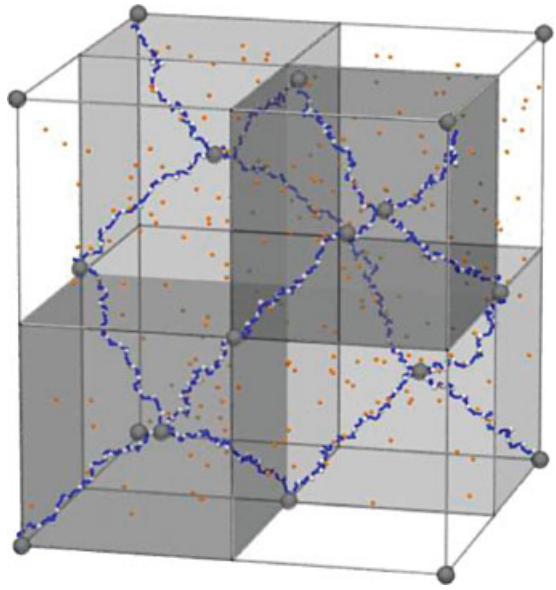

Figure 1.
Snapshot depicting the diamond lattice topology of the polyelectrolyte network. From the $N_{nodes} = 8$ tetra-functional nodes (for illustration purposes drawn as oversized gray spheres) $N_p = 16$ polymer chains emerge, on each fN_m monomers charged (white spheres) and (1 - f)N_m neutral (blue spheres). While they only occupy those four subboxes shaded in gray, the N_{CI} counterions (orange spheres) move freely through the entire unit cell.

© 2006 WILEY-VCH Verlag GmbH & Co. KGaA, Weinheim

for isothermal changes such as the adjustment of V if T remains constant due to the thermostat. Also requiring one (N, V, T)-simulation only, an external pressure P_{ext} is measured through an initial volume change from (P_α, V_α) to (P_β, V_β) as

$$\begin{aligned}(P_\alpha + P_{\text{ext}}) \cdot V_\alpha &= (P_\beta + P_{\text{ext}}) \cdot V_\beta \\ \Rightarrow \quad P_{\text{ext}} &= \frac{P_\beta V_\beta - P_\alpha V_\alpha}{V_\alpha - V_\beta}\end{aligned} \tag{2}$$

which allows to derive the targeted volume V_{j+1} (where $P_{j+1} = 0$ is assumed) from

$$\begin{aligned}(P_j + P_{\text{ext}}) \cdot V_j &= (0 + P_{\text{ext}}) \cdot V_{j+1} \\ \Rightarrow \quad V_{j+1} &= \frac{P_j + P_{\text{ext}}}{P_{\text{ext}}} \cdot V_j\end{aligned} \tag{3}$$

While this once again requires most accurate determination of the pressures involved, with P_{ext} entering all subsequent calculations here even more critical than before, it is nevertheless the fastest (N, V, T)-based method to find V_{eq}. Some improvements are also possible, e.g. moving from V_j to V_{j+1} in several smaller steps, which prevents the aforementioned danger of ruptured bonds or exploding systems, and re-calculating P_{ext} along the volume iterations[3].

In case of the poor solvent we had to determine $\mathcal{P}(V_{\text{eq}}) \approx 0$ from running a multitude of (N, V, T)-simulations which provided a $p(V)$-diagram of the given parameter set due to the much larger fluctuations the hydrophobic interactions introduced into the system. The reason why we also chose different parameters for the bond potential was to have our networks correspond to the very detailed simulational study of single polyelectrolyte chains in poor solvent conducted earlier by Limbach and Holm [60].

3.2 Pressure Contributions in Good Solvents

In a fully periodic system, the swelling equilibrium of a polymeric network is indicated by a vanishing total pressure $\mathcal{P} \approx 0$. This offers a well-defined starting point for both developing simple models describing e.g. the node-node separation R_{E} in that state and for investigating the interplay of the microscopic pressure contributions which reflect the respective relevance of the various interactions and correlations in the system.

3.2.1 Simple Scaling Arguments

Assuming the validity of FRH, the swelling equilibrium of a charged gel should mainly result from the elastic response of the chains' inner bonds balancing the osmotic pressure Π_{C} of the counterions trapped inside the network by the macroscopic electro-neutrality requirement. Treating the N_{CI} counterions as an ideal gas-like cloud surrounding the N_{p} chains, $\Pi_{\text{C}} = k_{\text{B}} T \frac{N_{\text{CI}}}{V} \propto k_{\text{B}} T \frac{fN_{\text{m}}}{R_{\text{E}}^3}$, and the presence of fN_{m} counterions stretches each chain as if a force f_{E} was acting on the ends, elongating it to an end-to-end distance R_{E}. Evidently, this can only be an accurate description as long as the coulombic contribution $\Pi_{\ell_{\text{B}}}$ to the pressure remains negligible, *i.e.* the N_{m} monomers per strand are not too strongly charged, the fraction $(1-f)$ of neutral ones is not too small, and the electrostatic interactions are not too large.

In that simplification, employing the classical tension blob model [65, 66] the network chains can be treated as a sequence of $\frac{N_{\text{m}}}{g}$ blobs of size $\xi = bg^{\nu}$ containing g monomers of size b each, resulting in $R_{\text{E}} = \xi \cdot \frac{N_{\text{m}}}{g}$ as the chain extension, where ξ is chosen such that one blob has the energy $k_{\text{B}}T = f_{\text{E}} \cdot \xi$. Hence, $\Pi_{\text{E}} = \frac{\cdot f_{\text{E}} \cdot R_{\text{E}}}{R_{\text{E}}^3} = \frac{k_{\text{B}}T}{R_{\text{E}}^3} \cdot \frac{N_{\text{m}}}{g}$ is supposed to balance the osmotic pressure Π_{C} of the counterions given above, so that the number of monomers per blob must read as $g = \frac{1}{f}$. The scaling prediction [52, 15, 16] for the network strands then yields

$$\begin{aligned}R_{\text{E}} &= f^{1-\nu} N_{\text{m}} b \quad \Rightarrow \\ \alpha_\nu &= \frac{R_{\text{E}}^2}{R_\nu^2} = (fN_{\text{m}})^{2(1-\nu)}\end{aligned} \tag{4}$$

using the single chain description $R_\nu = bN_{\text{m}}^\nu$ for uncharged systems in the swelling ratio α_ν. For Gaussian chains (θ-solvent, $\nu = \frac{1}{2}$) the very same result has been obtained [52,

[3] The latter, however, turns out to amplify roundoff errors in V_j and V_{j+1} dramatically.

© 2006 WILEY-VCH Verlag GmbH & Co. KGaA, Weinheim

53, 54] by simply balancing Π_C to $\Pi_E = -\frac{k_B T}{N_m b^2 \cdot R_E}$, so that the blob picture turns out to be an equivalent description; in a good solvent, however, $\nu = \frac{3}{5}$ [65] or $\nu = 0.588$ [67, 68, 69], hence the dependency of R_E on f is expected to be more pronounced than for the θ-case (note that $0 < f \leq 1$).

3.2.2 Counterion Condensation

As can be inferred from Figure 2, the assumption of an ideal gas-like distribution made in section 3.2.1 holds sufficiently well for weakly charged systems. Without electrostatics (*black lines*), all distributions coincide as expected after a successful equilibration of the systems, because then the number of neutral "counterions" should not be influential to their homogeneous spread throughout the network at a constant density; the excluded volume of the chains' monomers however introduces a constant shift from the shape of the pure ideal gas also given in the plot. While for $\ell_B = 1\sigma$ (*blue lines*) and $f \leq 0.25$ there is not much deviation from the uncharged cases observable, stronger electrostatics perturb the "cloud" of counterions surrounding the network chains, increasingly attracting the former towards the charged monomers on the strands. With the integrated distribution functions taking on an (initially) concave shape up to an inflection point (R_M, f_x) which will be discussed later on, counterion condensation sets in. In the plots, this is the case for $\ell_B = 5\sigma$ (*red lines*) and $f \geq 0.25$, although strong deviations from the ideal gas-like behaviour are already apparent for intermediate parameter regimes like $\ell_B = 5\sigma$ and $f = 0.125$ where 40% of the counterions are within a distance of $|r| = L/10$ around a network strand, illustrating the difficulty of defining something as continuous as this "condensation" effect which is obviously all but a sharp transition between two distinct phases or states.

3.2.3 Balance in the Pressure

One of the major advantages of computer simulations is the access to "microscopic" details of the investigated systems. Particularly in the case of far-reaching assumptions such as section 3.2.1 neglecting electrostatics entirely, it is beneficial to be able to actually compare the (theoretically) assumed behaviour to the (model) reality. Therefore, this section will investigate the contributions of counterions resp. gel to the overall pressure $\mathcal{P}$ by splitting it into its ideal components $\mathcal{P}^{Cl}_{ideal}$ and $\mathcal{P}^{monomers}_{ideal}$ of counterions and monomers, respectively, their excluded volume interactions with themselves ($\mathcal{P}^{Cl-Cl}_{LJ}$ and $\mathcal{P}^{monomers}_{LJ}$) and with each other ($\mathcal{P}^{Cl-monomers}_{LJ}$) from the Lennard-Jones interaction, the total electrostatic pressure ($\mathcal{P}^{tot}_{\ell_B}$) from the coulombic coupling, and the FENE-virial from the bonds ($\mathcal{P}_{FENE}$). Setting $\mathcal{P}^{Cl}_{LJ} = \mathcal{P}^{Cl-Cl}_{LJ} + \mathcal{P}^{Cl-monomers}_{LJ}$, these are grouped into

$$\mathcal{P}_{gas} = \mathcal{P}^{CI}_{ideal} + \mathcal{P}^{CI}_{LJ} + \mathcal{P}^{tot}_{\ell_B} \quad (5)$$

$$\mathcal{P}_{gel} = \mathcal{P}^{monomers}_{ideal} + \mathcal{P}^{monomers}_{LJ} + \mathcal{P}_{FENE} \quad (6)$$

with $\mathcal{P} = \mathcal{P}_{gas} + \mathcal{P}_{gel}$, representing the "pressure of the gas" and the "pressure of the gel", respectively.

Now, the theory in section 3.2.1 assumed electrostatics to be neglegible, which would correspond to $\mathcal{P}^{tot}_{\ell_B} \approx 0$, and the counterions to behave as an ideal gas, from where $\mathcal{P}^{Cl-Cl}_{LJ} \approx 0$ and $\mathcal{P}^{Cl-monomers}_{LJ} \approx 0$ would follow. Looking at the numbers it however turns out that this is only true for small charge fractions f (*i.e.* few counterions N_{Cl}) and weak coulombic coupling (*i.e.* small Bjerrum length ℓ_B). Otherwise the charges on the chains attract the free ions into forming a cloud layer around the strands. This phenomenon is also known from the study of charged rods [70] where a *Manning parameter* $\xi_M = \frac{\ell_B}{b/f} > \frac{1}{\nu_{Cl}}$ (ν_{Cl} being the valency of the counterions, $\nu_{Cl} = 1$ in our case) indicates that a fraction of $(1 - \frac{1}{\xi_M})$ counterions will "condense" onto the rod, *i.e.* will be confined to a small cylindrical volume around it, where they are neutralized such that f is renormalized towards an *effective charge fraction*

$$f_{eff} = \begin{cases} f & \text{for } \frac{\ell_B}{b/f} < \frac{1}{\nu_{Cl}} \Rightarrow f < f_{max}, \\ f_{max} = \frac{b}{\nu_{Cl}\ell_B} & \text{for } \frac{\ell_B}{b/f} \geq \frac{1}{\nu_{Cl}} \Rightarrow f \geq f_{max}. \end{cases} \quad (7)$$

© 2006 WILEY-VCH Verlag GmbH & Co. KGaA, Weinheim

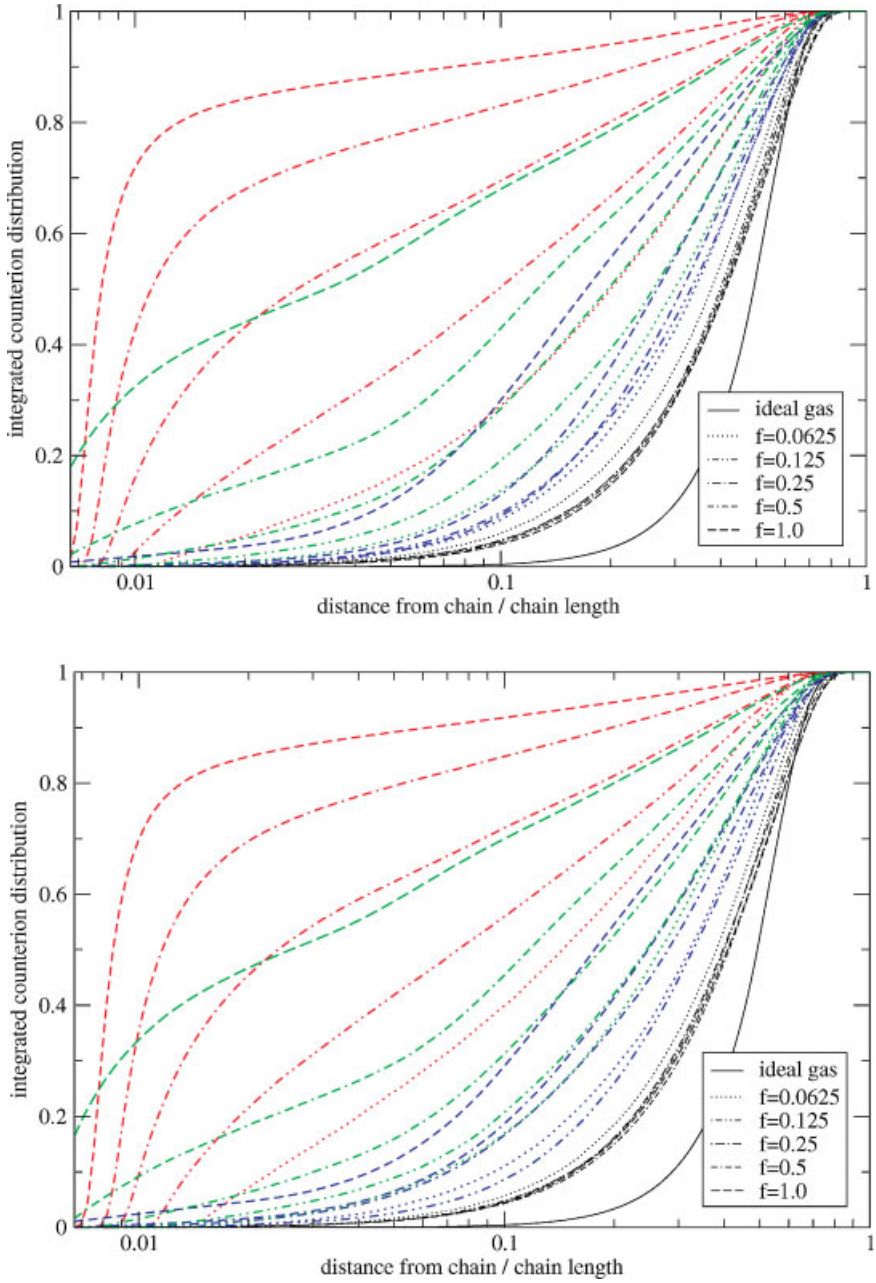

Figure 2.
Integrated counterion distribution for $N_m = 239$, with $\ell_B = 0\sigma$ (*black lines*), $\ell_B = 1\sigma$ (*blue lines*), $\ell_B = 2\sigma$ (*green lines*), and $\ell_B = 5\sigma$ (*red lines*) in good solvent (*top*) and close to the θ-point (*bottom*), normalized by the end-to-end distance $\langle R_E^2 \rangle^{1/2}$; different line style corresponds to different charge fractions *f* (see legend). For comparison, the corresponding ideal gas distribution for $\ell_B = 5\sigma$ and f = 1.0 is given as well (*solid black line*). Note that each of the systems has its own V_{eq}, the graphs therefore reach the horizontal axis at different $1/R_E$.

© 2006 WILEY-VCH Verlag GmbH & Co. KGaA, Weinheim

The remaining unperturbed ions may still behave similar to an ideal gas with reduced effective osmotic pressure $\Pi_C^{eff} \propto k_B T \frac{f_{eff} N_m}{R_E^3}$.

Transferring this depiction to the polyelectrolyte networks, we now expect the pressure balance to follow [15, 16]

$$\mathcal{P} \approx \Pi_C^{eff} + \Pi_E = P = 0$$

$$\Rightarrow R_E = N_m b \cdot f_{eff}^{1-\nu} \quad (8)$$

which is confirmed by our simulation data shown in Figure 3.

Note however that this result is only due to a fortituous cancellation of contributions, as the thorough analysis of the individual pressure components and their relation to the theoretically predicted behaviour shows [16] a strong cross-correlation between the subsets in (5) and (6). Consequently, though (8) offers an easy way of estimating the equilibrium swelling behaviour of a polyelectrolyte network, it is not to be taken as a description of the underlying physical mechanisms leading to that effect. There, the finite extensibility of the network chains as well as the self-energy repulsion of the like-wise charged monomers have an increasing impact on the final shape as have the excluded-volume interactions of the condensing counterions. For a full discussion see reference [71].

3.3 Network Conformations in Poor Solvents

A large number of polymers are based on a hydrocarbon backbone which is usually non-soluble in water. While quite often only the addition of charged side groups ensures solubility, the properties of such polyelectrolytes are fundamentally different than those of the macromolecules considered in the previous section 3.2. Since most polymers in biological environments, where the amount of water is usually high, virtually all proteins as well as the DNA are charged objects, the importance of this regime and its thorough understanding not only for biochemistry and molecular biology becomes apparent.

3.3.1 Appearances of Swollen Equilibrium

In a neutral system, hydrophobic interactions would immediately induce the collapse of a macromolecular object because by that the surface with the surrounding solvent could be minimized. For a charged polymer, however, the repulsion of the likewise charged repeat units introduces an additional effect counteracting the collapsing tendencies induced by the solvent, such

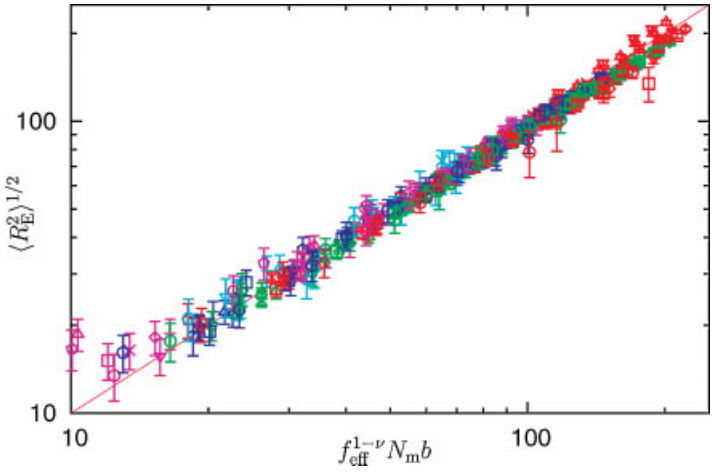

Figure 3.
The equilibrium swelling behaviour of salt-free polyelectrolyte networks in good solvent and close to the θ-point following the scaling law (8) successfully (same symbols refer to same Bjerrum length ℓ_B, same colour indicates same charge fraction).

© 2006 WILEY-VCH Verlag GmbH & Co. KGaA, Weinheim

that within certain parameter regimes a fragile balance can emerge, creating a sequence of locally collapsed structures (called *pearls*) interconnected by elongated strings, having the polyelectrolyte appear as a *pearl-necklace*. On the basis of fluorescence studies, similar necklace conformations have been proposed [72], while for weakly [73, 74, 75] and strongly [76, 77, 78] charged chains they have also been predicted by scaling theories. Albeit computer simulation studies [79, 80, 60] were successful in proving their existence within model systems, also providing valuable insight into their basic properties, direct experimental evidence is lacking so far, only first hints to their occurrence have been found [81, 82, 83, 84, 85]. This is not too surprising regarding the strong fluctuations pearl-necklace structures already exhibit in simulation systems; even despite the fact that all microscopic details are fully accessible, equilibrium state properties are consequently quite difficult to define and to measure. In a real world experiment, however, the same task is much more challenging, not least as there are even many more unwanted side effects, e.g. impurities of the solvent, polydispersity of the chains, defects in their conformation, and so on.

There is no apparent reason why similar structures observed for the single polyelectrolytes should not be present in our charged hydrogels as well, once they are placed in a poor solvent environment. In fact, for the formation of pearl-necklaces this was already postulated theoretically [53] if one assumes the strands between neighbouring network nodes to be sufficiently long. Using the same parameters as the single chain study by Limbach and Holm [60], we therefore investigated systems with $N_m = 199$ as chain length[4] and charge fraction $f \in \{0.125, 0.25, 0.3333, 0.5, 1.0\}$ for multiple Bjerrum lengths $\ell_B \in \{0\sigma, 0.125\sigma, 0.25\sigma, 0.5\sigma, 0.75\sigma, 1.0\sigma, 2.0\sigma, 3.0\sigma, 5.0\sigma, 6.0\sigma, 9.0\sigma\}$ with the network model introduced in section 3.1. Without the possibility to use the (N, p, T)-ensemble, the swelling equilibrium had to be determined from the roots[5] of a $p(V)$-diagram which relates the simulation box volume V to the pressure $\mathcal{P}$ measured according to (1) and averaged over uncorrelated network conformations.

From there, we investigated some simulation snapshots across the parameter space of charge fraction f and Bjerrum length ℓ_B, and did indeed find conformational structures similar to the single chain study [60]. Most predominantly we successfully identified a pearl-necklace regime, whose existence theorists started to suspect for charged hydrogels in poor solvent as well, once the corresponding conformations had been found for the single polyelectrolytes. The inset of Figure 4 shows such a prediction, taken from [53], and relates it to an actual snapshot from our simulation with much longer chains ($N_m = 479$) in the otherwise unchanged parameter regime (*i.e.* $f = 0.3333$ and $\ell_B = 1.5\sigma$) to emphasize that formation of more than one pearl is actually possible and is only dependent on the available chain length. Not only are the five to six small, collapsed globules visible along the network backbone, where the hydrophobicity of the monomers (drawn as *red spheres*) caused them to overcome their mutual electrostatic repulsion to minimize their respective contact surface with the (implicite) solvent surrounding the chains, while their thereby increased charge accumulation of each pearl ensures their arrangement as relatively rigid, linear necklaces, but the onset of counterion condensation is visible as well, seeing several of the ions (the *gray spheres*) close to the strands, and there particularly to the globules, betraying the otherwise gas-like distribution in the system.

For stronger electrostatics this will eventually lead to an entire, global collapse of the network, once the coulombic coupling attracts all counterions onto the

[4] In the case of $f = 0.3333$ the chain length was actually chosen to be $N_m = 200$ to ensure that $N_{CI} \in \mathbb{N}$.

[5] If there is more than one, we are looking at a phase transition in the volume.

© 2006 WILEY-VCH Verlag GmbH & Co. KGaA, Weinheim

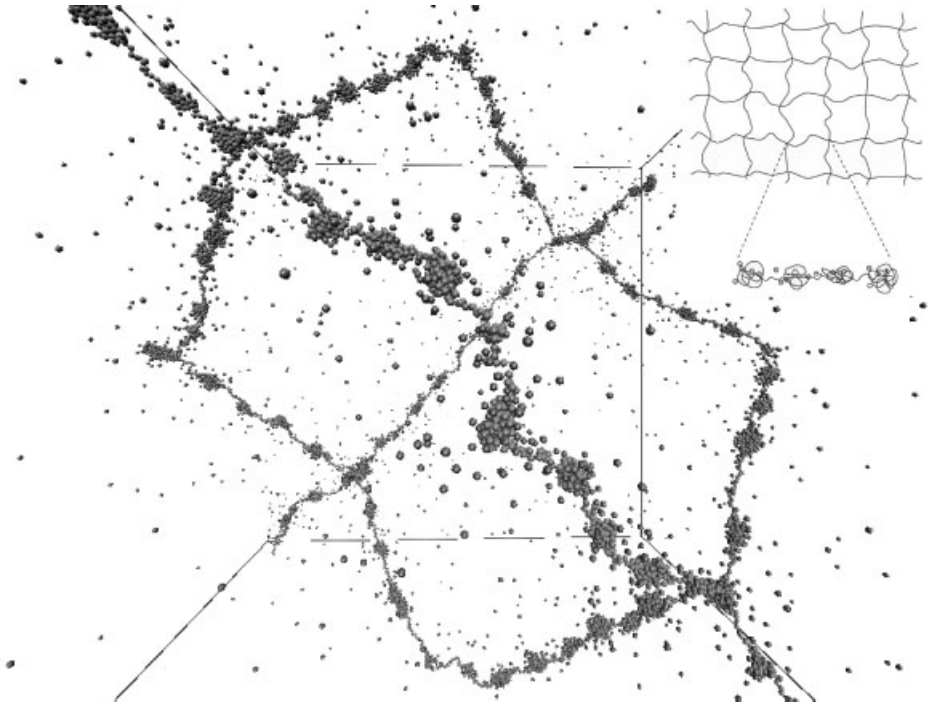

Figure 4.
Snapshot of an equilibrium conformation for $N_m = 479$, f = 0.3333, and $\ell_B = 1.5\sigma$, nicely depicting the predicted pearl-necklace structure the theoretical sketch in the inset (taken from Vilgis *et al.*) envisioned.

chains, essentially neutralizing everything such that the hydrophobicity takes over. Before that happens, there will be an intermediate regime of strong ionic interactions which has either the repulsion of the like-wise charged counterions win, resulting in highly swollen hydrogels once the osmotic pressure of the ions dissolved all globules on the strands and occuring for high charge fractions f, or the condensation effects dominate (for lower f and larger ℓ_B) such that the pearls coalesce towards thick network arms composed of multi-layered monomer sequences.

In the opposing case of only few counterions (*i.e.* small fraction f) the hydrophobic interactions are always stronger than the coulombic coupling, independent of ℓ_B. The only effect electrostatics then has is limited to short-range order, if monomers and counterions are phase-separated to maximize monomeric contacts (small ℓ_B) or if they are mixed to maximize charge compensation (high ℓ_B).

Figure 5 summarizes these results by illustrating regimes of common conformations i.e., collapsed conformations for small charge fractions or very strong electrostatics, pearl-necklaces for moderate to high charge fractions and not too strong coulombic coupling, stretched structures for large f and moderate ℓ_B, and finally the ''sausage''-regime for larger Bjerrum lengths; to emphasize the trends, it distinguishes between cases where only the nodes act as condensation nuclei, and those with at least one additional pearl along the network strand.

Compared to the single chains we notice that the structure diagram for polyelectrolyte networks contains similar regimes, albeit at shifted positions in the parameter space, despite the fact that we used the very same set of parameters for our simulations. Besides the pearl-necklace regime extending down to the case of vanishing electrostatics ($\ell_B = 0\sigma$) for not too low charge fractions, we do not (and cannot) find

© 2006 WILEY-VCH Verlag GmbH & Co. KGaA, Weinheim

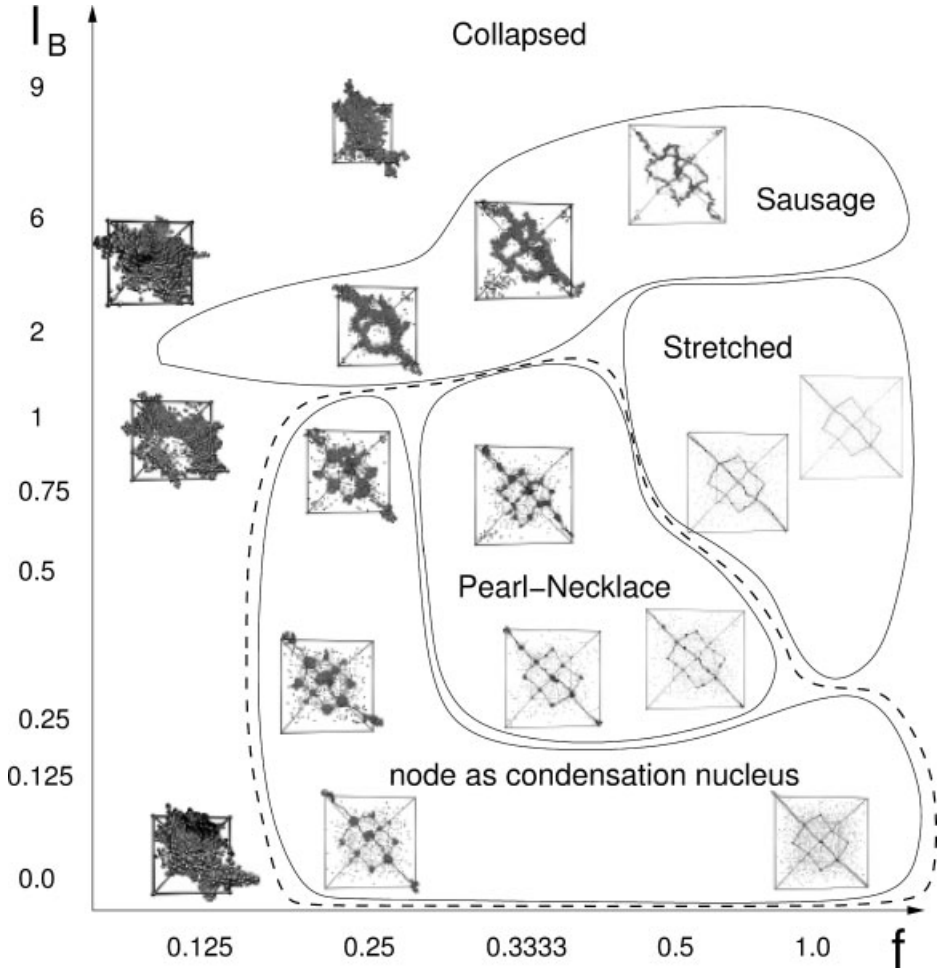

Figure 5.
Structure diagram of the equilibrium swelling conformations charged hydrogels assume in a poor solvent with $\varepsilon_{LJ} = 1.75\, k_B T$ for varying charge fraction f and Bjerrum length ℓ_B, contrasting the corresponding picture for single polyelectrolytes by Limbach and Holm.

globular conformations, both differences due to the network topology trapping the counterions. Once electrostatics is up and chains are sufficiently long, the charged hydrogels behave similarly to the single polyelectrolytes, including the collapse for very strong coulombic coupling where the remaining dependence on the network topology becomes negligible. As we have ventured further towards lower charge fractions, also investigating $f = 0.25$ and $f = 0.125$ which were not considered in the single chain study, we are able to conclude on that limit, too, particularly since we find only collapsed conformations for the lowest amount of counterions which are obviously insufficient to generate a strong enough osmotic pressure to push the attractive monomers apart. (One would consequently expect single polyelectrolytes with $f = 0.125$ to also form globules for all values of ℓ_B, with an increasing amount of counterion condensation and subsequent mixing between ions and monomers for growing electrostatics, arguing that the few remaining charges on the chain are not sufficient to effectively counteract the collapsing tendencies).

© 2006 WILEY-VCH Verlag GmbH & Co. KGaA, Weinheim

In general, the parameter space for polyelectrolytes has far more dimensions, such as the solvent quality parameter ε_{LJ}, the valency of monomers or counterions, and added salt in the system. As we are focusing on a direct comparison with the single chain results, none of these were examined further; for the future, however, they would provide the next logical steps.

3.3.2 Form Factor Findings

More information about the chain conformation is usually obtainable from the form factor $S(q)$, which is obtainable from both experiment and computer simulation without too much effort, making it an ideal tool to compare real world results with numerical modeling. For the single polyelectrolytes, the form factor of the chains with $N_m = 382$ in the study of Limbach and Holm [60] is plotted on the *left* of Figure 6, where it is known that they assume pearl-necklace conformations with $n_P = 4.5$ pearls per chain; it is compared to the charged hydrogels of our investigations plotted on the *right* for the chain lengths between $N_m = 335$ and $N_m = 479$, exhibiting $n_P = 4.0$, $n_P = 4.3$, $n_P = 5.9$, $n_P = 5.7$ pearls, respectively.

In the Guinnier regime of low scattering angles $qR_G \ll 1$, the form factor can be expanded [86] into the *Guinnier function*

$$S(q) \approx N_m exp\left(-\frac{q^2 R_G^2}{3}\right) \approx N_m\left(1 - \frac{q^2 R_G^2}{3}\right) \quad (9)$$

providing a basis for determining the radius of gyration from small-angle scattering experiments for objects with unknown form factor. This yields $R_G = 16.8\sigma$ for the single polyelectrolytes, in good agreement with the directly measured $R_G = 16.9\,\sigma$ [60], while in case of the charged hydrogels the same approach results in $R_G = 16.7\,\sigma$ for the network chains with $N_m = 383$ monomers, which is also corresponding quite perfectly to the $R_G = 16.7\sigma$ observed; the other network chains also lead to matching values of $R_G = 15.8\,\sigma$ (for $N_m = 335$), $R_G = 17.2\sigma$ ($N_m = 431$), and $R_G = 17.7\sigma$ ($N_m = 479$) for both types of derivations.

Small scattering angles between $0.07\sigma^{-1}$ and $0.4\,\sigma^{-1}$ see the form factor scale as $S(q) \propto q^{-1}$, reminiscent of the strongly elongated structures we observed for good solvent hydrogels; on length scales larger than 15σ the chain conformations are therefore stretched. It should however be noted that for the isolated polyelectrolytes this behaviour is only approximately reached, indicated by the employed fit of $\sim q^{-0.93}$ in the plot, whereas the charged hydrogels clearly exhibit an almost perfect match with $\sim q^{-1.00}$ over the entire range given. This reflects what we already found earlier in the characteristic ratio $r = \langle R_E^2 \rangle / \langle R_G^2 \rangle$ where the single chains could not really reach the rod-like regime of $r = 12$ while the networks even exceeded that threshold locally; it also emphasizes the influence of the node connectivity which is the responsible mechanism.

For wave vectors around $q \approx 0.5^{-1}\sigma$, we observe a weakly pronounced shoulder in the form factor. Looking closer (see inset of Figure 6) it is revealed that $S(q)$ has an inflection point there, which could be related to the inter-pearl scattering in [60].

In the limit of large q between $0.9\sigma^{-1}$ and $2.5\sigma^{-1}$, the scaling shifts towards $S(q) \propto q^{-4}$, the typical Porod scattering of strongly collapsed objects. While the single polyelectrolytes exhibit another small dip at $q \approx 1.7\sigma^{-1}$ which relates to the pearl radius, the networks do not seem to distinctly have such a feature because of the external tension exerted through the network topology.

The cooperative effect of fluctuations on overlapping length scales consequently broadens all characteristic signatures that can be revealed by experimental scattering methods. Considering that we have investigated a model system without impurities, irregularities, influences of defects or other obstructions to the leading mechanisms we identified here, pear-necklace structures might indeed be difficult to detect in real world experiments. Nevertheless, our computer simulations allowed to indicate some

© 2006 WILEY-VCH Verlag GmbH & Co. KGaA, Weinheim

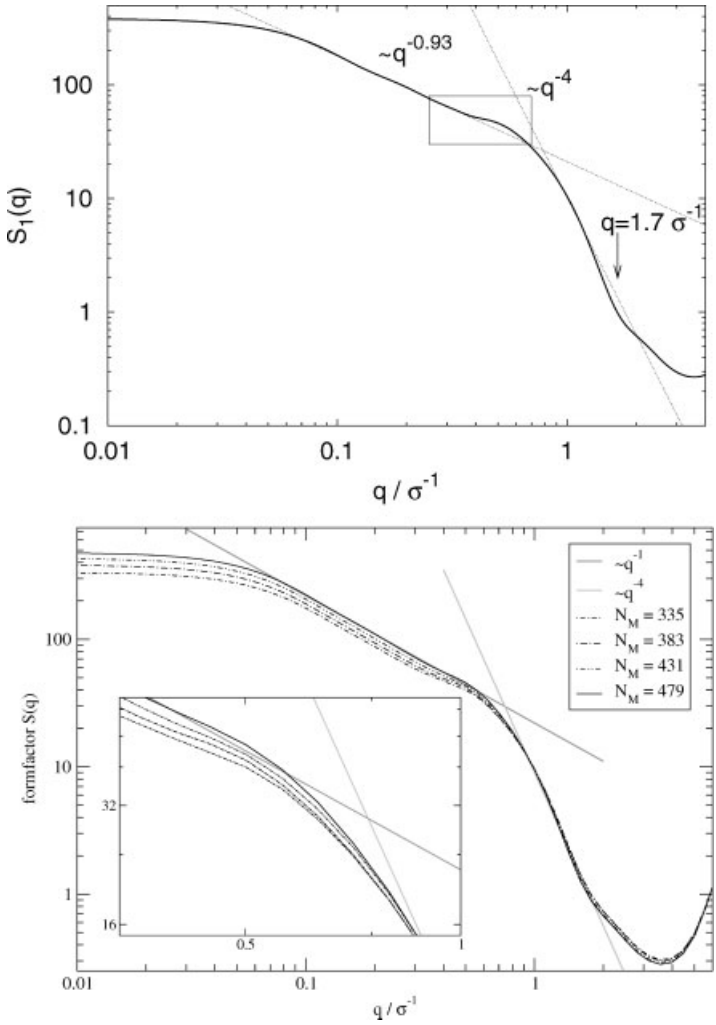

Figure 6.
Form factor S(q) for typical pearl-necklace conformations on single polyelectrolytes (*top*, taken from Limbach and Holm) with $N_m = 382$, $f = 0.3333$, $\ell_B = 1.5\sigma$, and for networks (*bottom*) with the same parameters but different chain lengths; the straight lines are fits to certain *q*-ranges, the marked region indicates a shoulder in the plots present for both systems which is magnified in case of the hydrogels.

of the prominent features experimentalists can expect when analyzing their data, which combined with highly regular model networks such as the example of P*t*BMA [87] should finally enable experimental observation of the prominent pearl-necklace structures unique to polyelectrolyte networks in poor solvent.

Acknowledgements: We are grateful to the many people who contribute(d) to the (still ongoing) development process of ESPResSo, see http://www.espresso.mpg.de for further details. This work was supported by the German Science Foundation through SFB 625 and by the Cusanuswerk. Helpful discussions and valuable remarks by R. Everaers, M. Deserno, B. Dünweg are gratefully acknowledged. Special thanks go to T. Schürg for his help with the simulation box snapshots.

[1] A. Arnold, B. A. Mann, H.-J. Limbach, and C. Holm, in *Forschung und wissenschaftliches Rechnen 2003*, Vol. *63* of *GWDG-Bericht*, edited by K. Kremer and V. Macho

© 2006 WILEY-VCH Verlag GmbH & Co. KGaA, Weinheim

(Gesellschaft für wissenschaftliche Datenverarbeitung mbh, Göttingen, Germany, 2004), pp. 43–59.
[2] H.-J. Limbach, A. Arnold, B. A. Mann, and C. Holm, comp. Phys. Comm., in press (unpublished).
[3] R. A. L. Jones, *Soft Condensed Matter* (Oxford University Press, Great Clarendon Street, Oxford OX2 6DP, 2002).
[4] L. Treloar, *The Physics of Rubber Elasticity* (Clarendon Press, Oxford, 1986).
[5] *Electrostatic Effects in Soft Matter and Biophysics*, Vol. *46* of *NATO Science Series II -Mathematics, Physics and Chemistry*, edited by C. Holm, P. Kékicheff, and R. Podgornik (Kluwer Academic Publishers, Dordrecht, Nl, 2001).
[6] M. J. Stevens and K. Kremer, J. Chem. Phys. **103**, 1669 (1995).
[7] C. Holm, in *Computational Soft Matter: From Synthetic Polymers to Proteins*, Vol. *23* of *NIC series*, edited by N. Attig, K. Binder, H. Grubmüller, and K. Kremer (Research Centre Jülich, ADDRESS, 2004).
[8] A. Arnold and C. Holm, in *Advanced Computer Simulation Approaches for Soft Matter Sciences*, Vol. *II* of *Advances in Polymer Sciences*, edited by C. Holm and K. Kremer (Springer, ADDRESS, 2005, in press).
[9] J. Norberg and L. Nilsson, Quarterly Reviews of Biophysics **36**, 257 (2003).
[10] M. Deserno and C. Holm, J. Chem. Phys. **109**, 7678 (1998).
[11] M. Deserno and C. Holm, J. Chem. Phys. **109**, 7694 (1998).
[12] A. Arnold and C. Holm, Comp. Phys. Comm. **148**, 327 (2002).
[13] A. Arnold, J. de Joannis, and C. Holm, J. Chem. Phys. **117**, 2496 (2002).
[14] J. de Joannis, A. Arnold, and C. Holm, J. Chem. Phys. **117**, 2503 (2002).
[15] B. A. Mann, R. Everaers, C. Holm, and K. Kremer, Europhys. Lett. **17**, 786 (2004).
[16] B. A. Mann, C. Holm, and K. Kremer, J. Chem. Phys. **122**, 154903 (2005).
[17] W. Tschöp *et al.*, Acta Polymer. **49**, 61 (1998).
[18] W. Tschöp *et al.*, Acta Polymer. **49**, 75 (1998).
[19] K. Kremer and F. Müller-Plathe, Mol. Sim. **28**, 729 (2002).
[20] Tcl/Tk, Tool Command Language/ToolKit – Homepage, 2003.
[21] D. C. Rapaport, *The Art of Molecular Dynamics Simulation*, 2nd ed. (Cambridge University Press, ADDRESS, 2004).
[22] D. Frenkel and B. Smit, *Understanding Molecular Simulation*, 2nd ed. (Academic Press, San Diego, 2002).
[23] N. Martys and R. Mountain, Phys. Rev. E **59**, 3733 (1999).
[24] F. Müller-Plathe, Phys. Rev. E; **59**, 4894 (1999).
[25] T. Soddemann, B. Dünweg, and K. Kremer, Phys. Rev. E **68**, 046702 (2003).
[26] H. J. C. Berendsen*et al.*, J. Chem. Phys. **81**, 3684 (1984).
[27] P. Español and P. Warren, Europhys. Lett. **30**, 191 (1995).
[28] A. Kolb and B. Dünweg, J. Chem. Phys. **111**, 4453 (1999).
[29] I. R. Cooke, K. Kremer, and M. Deserno, submitted cond (2004).
[30] A. Arnold and C. Holm, Chemical Physical Letters **354**, 324 (2002).
[31] A. Arnold and C. Holm, in preparation (unpublished).
[32] K. S. Kazanskii and S. A. Dubrovskii, Adv. Polym. Sci. **104**, 97 (1992).
[33] F. Buchholz and N. Peppas, in *ACS Symposium Series*, American Chemical Society, edited by M. Comstock (American Chemical Society, Washington, D.C., 1994), Vol. *573*.
[34] G. M. Eichenbaum *et al.*, Macromolecules **32**, 4867 (1999).
[35] N. A. Peppas, P. Bures, W. Leobandung, and H. Ichikawa, Biopharm. **50**, *27* (2000).
[36] *Physical Chemistry of Polyelectrolytes*, Vol. *99* of *Surfactant Science Series* (Marcel Dekker Inc., New York, 2001).
[37] W. E. Rudzinski*et al.*, Design Monom. Polym. **5**, 39 (2002).
[38] J.-L. Barrat and J.-F. Joanny, Advances in Chemical Physics **94**, 1 (1996).
[39] A. Khokhlov, S. G. Starodubtzev, and V. V. Vasilevskaya, in *Conformational transitions in polymer gels: theory and experiment*, Vol. *109* of *Adv. Polym. Sci.*, edited by K. Dusek (Springer Verlag, New York, 1993), p. 123.
[40] W. Kuhn, B. Hargitay, A. Katchalsky, and H. Eisenberg, Nature **165**, 514 (1950).
[41] T. Tanaka, Phys. Rev. Lett. **40**, 820 (1978).
[42] K. Dusek, *Advances in Polymer Sciences* (Springer-Verlag, New York, 1993), Vol. *109* and *110*.
[43] A. Katchalsky and I. Michaeli, J. Polym. Sci. **15**, 69 (1955).
[44] I. Michaeli and A. Katchalsky, J. Polym. Sci. **23**, 683 (1957).
[45] P. Hansson, Langmuir **14**, 2269 (1998).
[46] H. S. Ashbaugh, L. Piculell, and B. Lindman, Langmuir **16**, 2529 (2000).
[47] J. Sjöström and L. Piculell, Colloids Surf. A **183–185**, 429 (2001).
[48] P. Hansson, S. Schneider, and B. Lindman, Prog. Colloid Polym. Sci. **115**, 342 (2000).
[49] P. Hansson, S. Schneider, and B. Lindman, J. Phys. Chem. B **106**, 9777 (2002).
[50] A. Fernandez-Nieves, A. Fernandez-Barbero, B. Vincent, and F. J. de las Nieves, Macromolecules **33**, 2114 (2000).
[51] A. Fernandez-Nieves, A. Fernandez-Barbero, B. Vincent, and F. J. de las Nieves, Prog. Colloid Polym. Sci. **115**, 134 (2000).
[52] J.-L. Barrat, J.-F. Joanny, and P. Pincus, J. Phys. II France **2**, 1531 (1992).

© 2006 WILEY-VCH Verlag GmbH & Co. KGaA, Weinheim

[53] T. A. Vilgis, A. Johner, and J.-F. Joanny, Eur. Phys. J. E **3**, 237 (2000).
[54] A. Khokhlov, K. Zeldovich, and E. Kramarenko, in *Electrostatic Effects in Soft Matter and Biophysics*, Vol. *46* of *NATO Science Series II -Mathematics, Physics and Chemistry*, edited by C. Holm, P. Kékicheff, and R. Podgornik (Kluwer Academic Publishers, Dordrecht, Nl, 2001), pp. 283–317.
[55] S. Schneider and P. Linse, Eur. Phys. J. E **8**, 457 (2002).
[56] Z.-Y. Lu and R. Hentschke, Phys. Rev. E **67**, 061807 (2003).
[57] Q. Yan and J. J. de Pablo, Phys. Rev. Lett. **91**, 018301 (2003).
[58] S. Schneider and P. Linse, J. Phys. Chem. B **107**, 8030 (2003).
[59] B. A. Mann, C. Holm, and K. Kremer, in preparation (2005).
[60] H. J. Limbach and C. Holm, J. Phys. Chem. B **107**, 8041 (2003).
[61] U. Micka, C. Holm, and K. Kremer, Langmuir **15**, 4033 (1999).
[62] U. Micka and K. Kremer, Europhys. Lett. **49**, 189 (2000).
[63] M. Deserno, Ph.D. thesis, Universität Mainz, 2000.
[64] G. S. Grest and K. Kremer, Phys. Rev. A **33**, 3628 (1986).
[65] P. Flory, *Principles of Polymer Chemistry* (Cornell University Press, Ithaca, NY, 1953).
[66] P. de Gennes, *Scaling Concepts in Polymer Physics* (Cornell University Press, Ithaca, NY, 1979).
[67] J. Zinn-Justin, *Quantum Field Theory and Critical Phenomena*, 2nd ed. (Clarendon Press/Oxford Science Publications, Oxford, 1993).
[68] B. Li, N. Madras, and A. Sokal, J. Stat. Phys. **80**, 661 (1995).
[69] A. Sokal, in *Monte Carlo and Molecular Dynamics Simulations in Polymer Science*, edited by K. Binder (Oxford University Press, New York/Oxford, 1995).
[70] G. Manning, J. Chem. Phys. **51**, 924 (1969).
[71] B. A. Mann, Ph.D. thesis, Johannes Gutenberg-University, Mainz, Germany, 2005.
[72] K.P. Ghiggino and K.L. Tan, in *Polymer photophysics*, edited by D. Phillips (Chapman and Hall, London; New York, 1985), Chap. 7, pp. 341–375.
[73] Y. Kantor, M. Kardar, and H. Li, Phys. Rev. E **49**, 1383 (1994).
[74] Y. Kantor and M. Kardar, Phys. Rev. E **51**, 1299 (1995).
[75] A. V. Dobrynin, M. Rubinstein, and S. P. Obukhov, Macromolecules **29**, 2974 (1996).
[76] H. Schiessel and P. Pincus, Macromolecules **31**, 7953 (1998).
[77] H. Schiessel, Macromolecules **32**, 5673 (1999).
[78] A. V. Dobrynin and M. Rubinstein, Macromolecules **32**, 915 (1999).
[79] H. J. Limbach and C. Holm, Comp. Phys. Comp. **147**, 321 (2002).
[80] H. J. Limbach, C. Holm, and K. Kremer, Europhys. Lett. **60**, 566 (2002).
[81] W. Essa, F. Lafuma, and C. E. Williams, J. Phys. II **5**, 1269 (1995).
[82] C. Heitz, M. Rawiso, and J. François, Polymer **40**, 1637 (1999).
[83] M. Heinrich*et al.*, Eur. Phys. J. E **4**, 131 (2001).
[84] D. Hinderberger, 2004, private communication.
[85] J. Combet, M. Rawiso, and F. Boué, 2005, in preparation.
[86] M. Rubinstein and R. H. Colby, *Polymer Physics* (Oxford University Press, Oxford, UK, 2003).
[87] C. Mengel, W. H. Meyer, and G. Wegner, Macromol. Chem. Phys. **202**, 1138 (2001).

© 2006 WILEY-VCH Verlag GmbH & Co. KGaA, Weinheim